

Electronic Supplementary Material (ESI) for New Journal of Chemistry

# A High-performance Regenerated Graphite Extracted from Discarded Lithium-ion Batteries

Dingshan Ruan,<sup>a,b,‡</sup> Fengmei wang,<sup>\*b,‡</sup> Lin Wu,<sup>b</sup> Ke Du,<sup>a</sup> Zhenhua Zhang,<sup>b</sup> Ke Zou,<sup>b</sup> Xiaofeng Wu,<sup>b</sup> Guorong Hu<sup>\*a</sup>

a School of Metallurgy and Environment, Central South University, Changsha 410083, P. R. China.

b Guangdong Brunp Recycling Technology Co., Ltd., Foshan 528100, P. R. China.

‡ These authors contributed equally to this work (D. S. Ruan and F. M. Wang)

\* Corresponding author. Tel & Fax: 13908482734; 15706429930

E-mail address: 1044283793@qq.com; wfm0127@163.com

## Experimental section

**Materials** Ptich which are used as the carbon source to coat on the surface of graphite was purchased from Jining lu coal-chemical Co., Ltd.,. Sulphuric acid (H<sub>2</sub>SO<sub>4</sub>, 98 %) was purchased from Xilong Scientific Co., Ltd.,. Commercial graphite (CGT, AML400) was purchased from

Dongguan Kaijin new energy Polytron Technologies Inc. Scrapped graphite (SGT) were taken from Guangdong Brunp Recycling Technology Co., Ltd.,. In detail, the discarded Li-ion batteries were discharged fully in a salt solution, and the dissolved toxic and corrosive species in waste salt solution such as LiOH could be reacted with  $\text{Na}_2\text{CO}_3$  for precipitation and recycling. And then those full-discharged discarded Li-ion batteries were mechanical broken to fragments. After treating at 500 °C in air atmosphere to removing the most of organic composition, Al and Cu which were acted as current collectors in discarded Li-ion batteries and steels used as the battery shells were screening by screen with the size of 100 mesh. Next, the different components (e.g. electrode materials and the residual celgard membrane) were selective separation using a DF-31AG pneumatic separator according to the difference in their densities. Finally, SGT was obtained after leaching out valuable metals by hydrometallurgical processes. All chemicals were used as recieved without further purification.

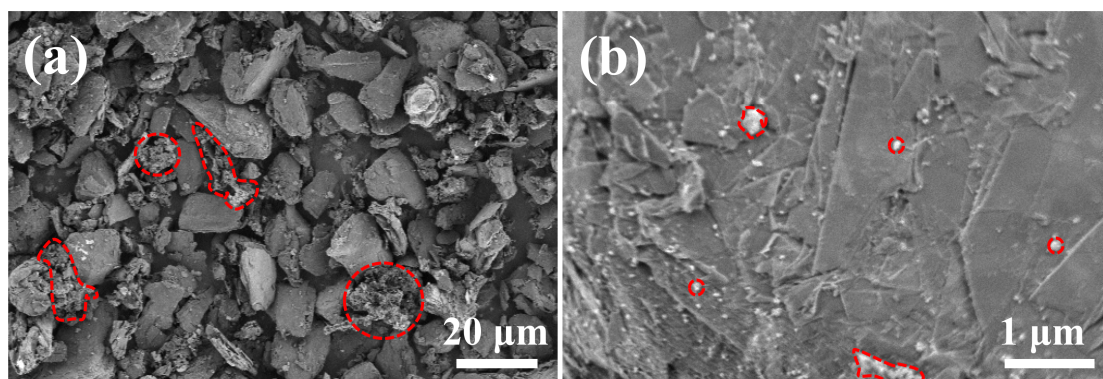


**Fig. S1** (a, b) SEM images with different magnifications of SGT

As shown in **Fig. S1a** and **b**, there are many impurities in SGT which may be electrochemical inactivity.

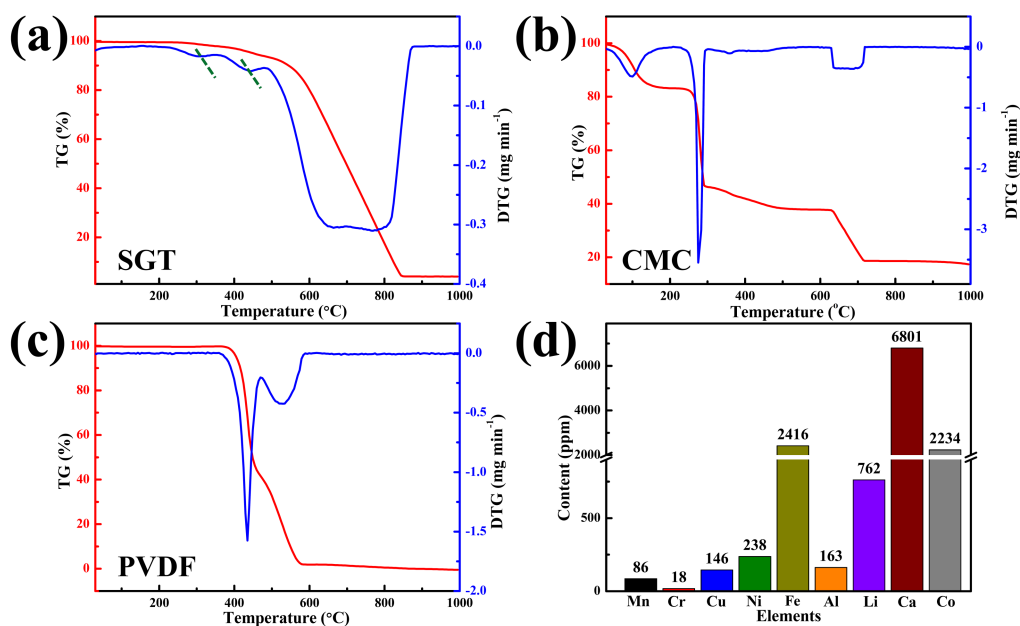


**Fig. S2** TG (Red) and DTG (Blue) curves of (a) SGT, (b) CMC and (c) PVDF; (d) The elemental analysis of SGT.

As shown in **Fig. S2a-c**, CMC and PVDF which were acted as the binder in LIBs are the main organic impurities in SGT demonstrating by thermogravimetric analysis. Besides, there are also many residual metal elements in SGT including Co, Li, Fe, Ni, Mn and Al shown in **Fig. S2d**.

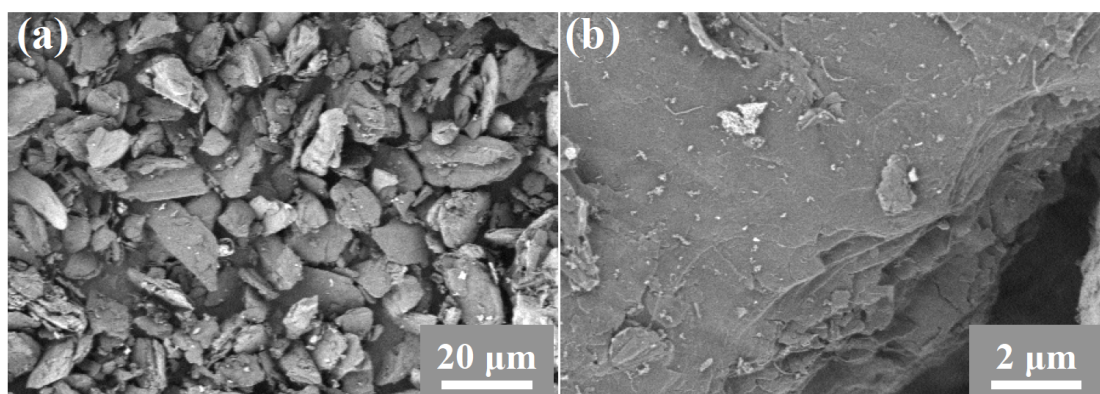


**Fig. S3** (a, b) SEM images with different magnifications of A-T-SGT.

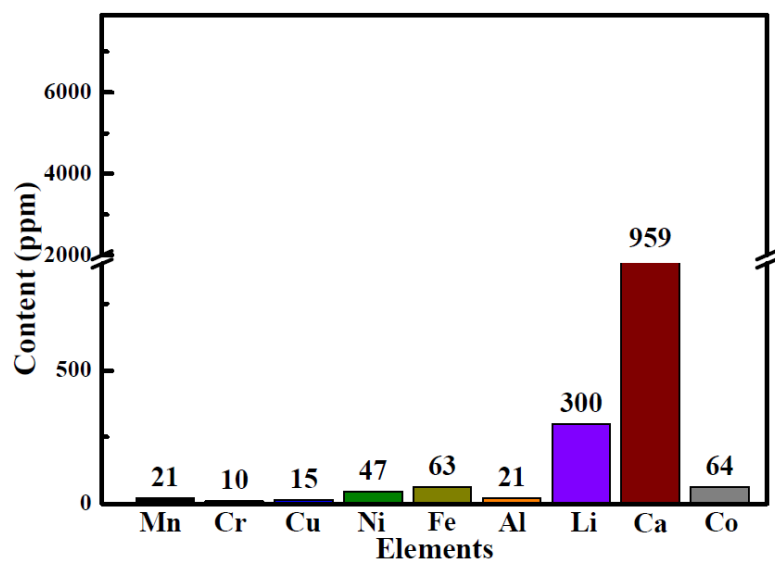


**Fig. S4** The elemental analysis of A-T-SGT.

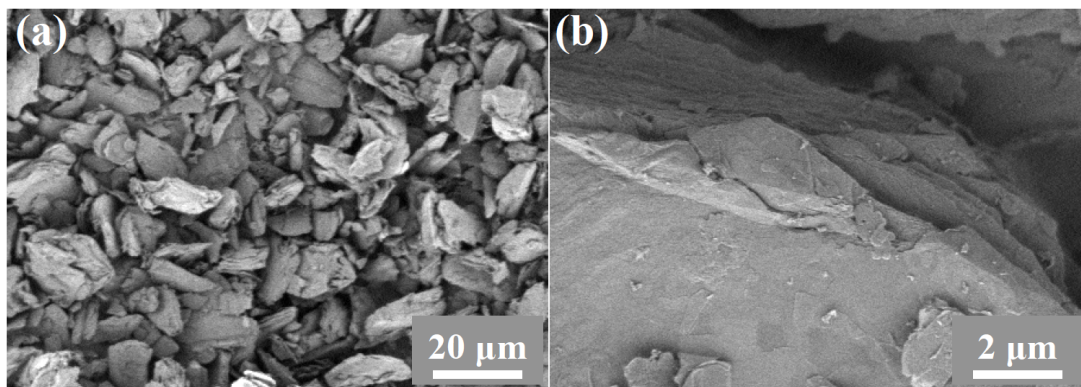


**Fig. S5** (a, b) SEM images with different magnifications of G-A-T-SGT.

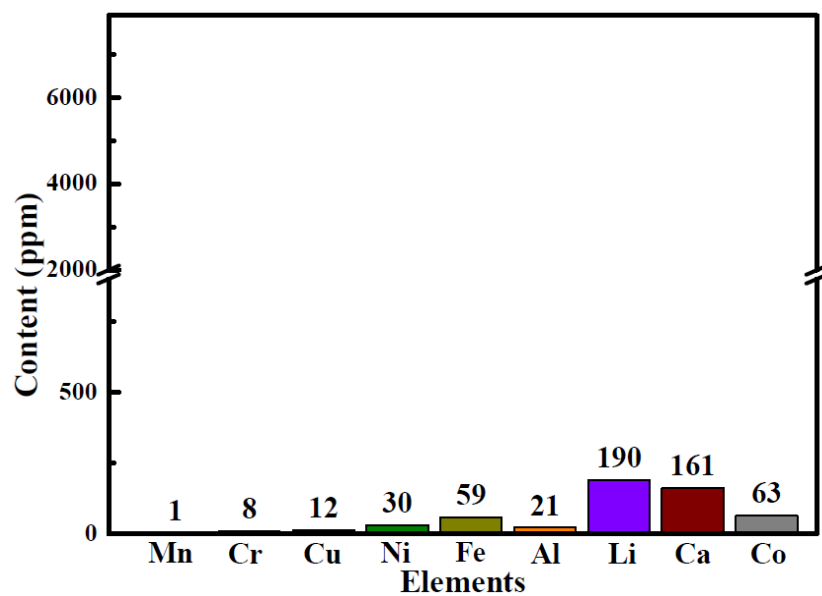


**Fig. S6** The elemental analysis of G-A-T-SGT.

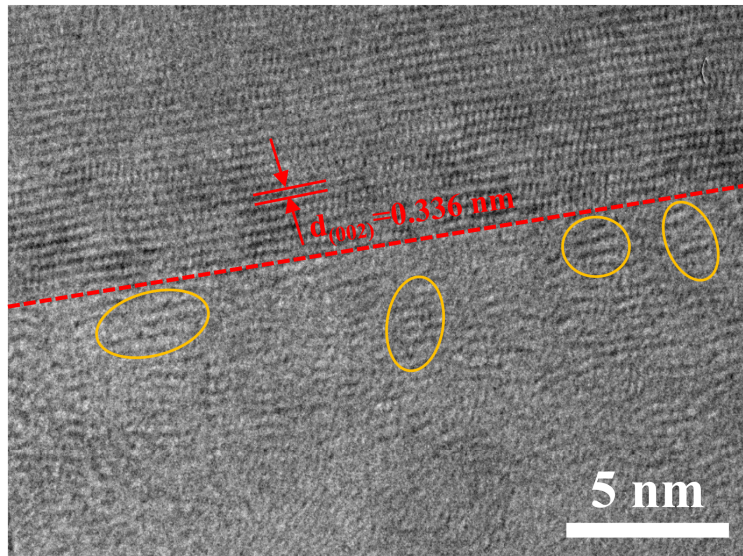


**Fig. S7** HRTEM image of G-A-T-SGT@C.

As shown in **Fig. S7**, lattice fringes with an interplanar spacing of  $\sim 0.336 \text{ nm}$  can be clearly observed upon the red imaginary line, corresponding to the (002) plane of graphite. Nevertheless, only a little of graphite crystallites can be detected under the red imaginary line which is the matched with the structure of amorphous carbon.

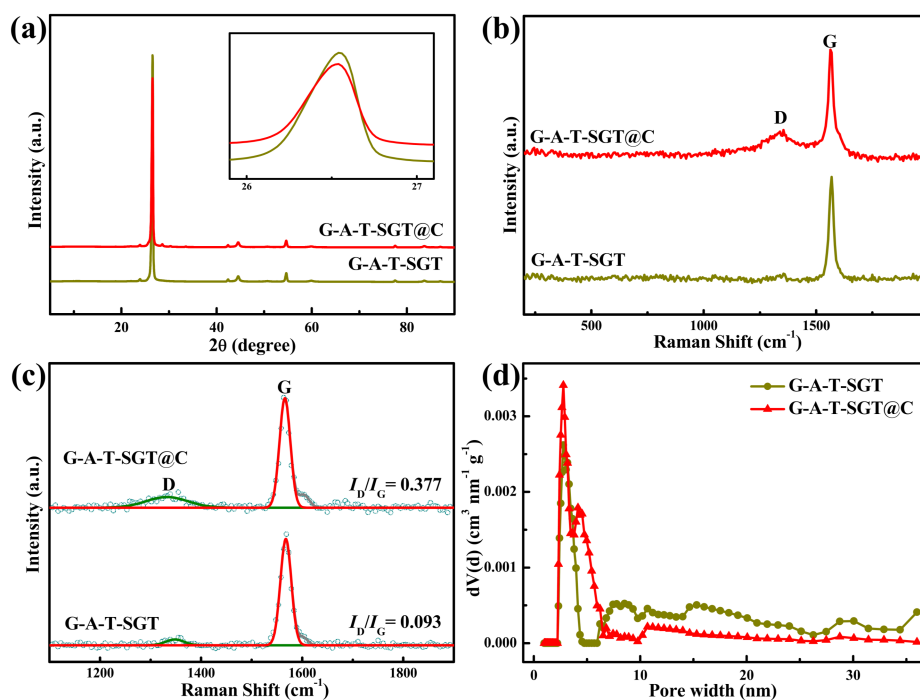


**Fig. S8** (a) XRD patterns, (b) Raman spectra, (c) Selected enlarged Raman spectra portion and (d) the pore size distribution of G-A-T-SGT and G-A-T-SGT@C.

As shown in **Fig. S8a**, the analogous XRD patterns of G-A-T-SGT and G-A-T-SGT@C indicate that the typical structure of graphite does not be destroyed during the coating process. Nevertheless, it is worth mentioning that the (002) peak intensity at around  $26.5^\circ$  of G-A-T-SGT@C is obviously lower than that of G-A-T-SGT which is attributed to the amorphous carbon layer covering on the surface of graphite. And the difference of  $I_D/I_G$  ratio between G-A-T-SGT@C (0.377) and G-A-T-SGT (0.093) shown in **Fig. S8c** is caused by the coating layer on the surface of G-A-T-SGT, attesting that the amorphous carbon derived from pitch is successfully coated on the surface of G-A-T-SGT. In addition, as shown in **Fig. S8d**, the pore at 6.5 ~ 35 nm is absence in G-A-T-SGT@C, in sharp contrast with G-A-T-SGT, which exhibit the similar tendency of pore texture with SGT but with obvious decrease of pore volume, confirming that the mesopore around 6.5 ~ 35 nm in G-A-T-SGT has been filled by amorphous carbon which will open up the transport channels of lithium ion and enhance the cycling performance and rate capability of LIBs.

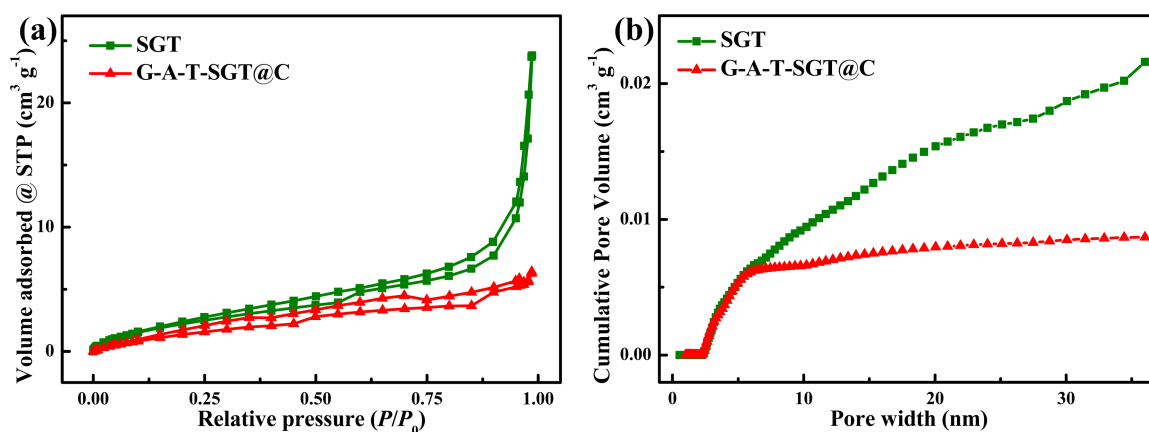


**Fig. S9** (a) N<sub>2</sub> adsorption-desorption isotherms and (b) the cumulative pore volume of SGT and G-A-T-SGT@C.

As shown in **Fig. S9a**, the N<sub>2</sub> adsorption/desorption isotherms of SGT and G-A-T-SGT@C display the typical type V curves with a specific hysteresis loops, indicating that the pore structures main are mesopore. And the total pore volume of G-A-T-SGT@C is smaller than that of SGT (**Fig. S9b**), indicating that most of defects of mesopore of SGT has been eliminated by pyrolyzation, acid leaching, graphitization and coating modification.

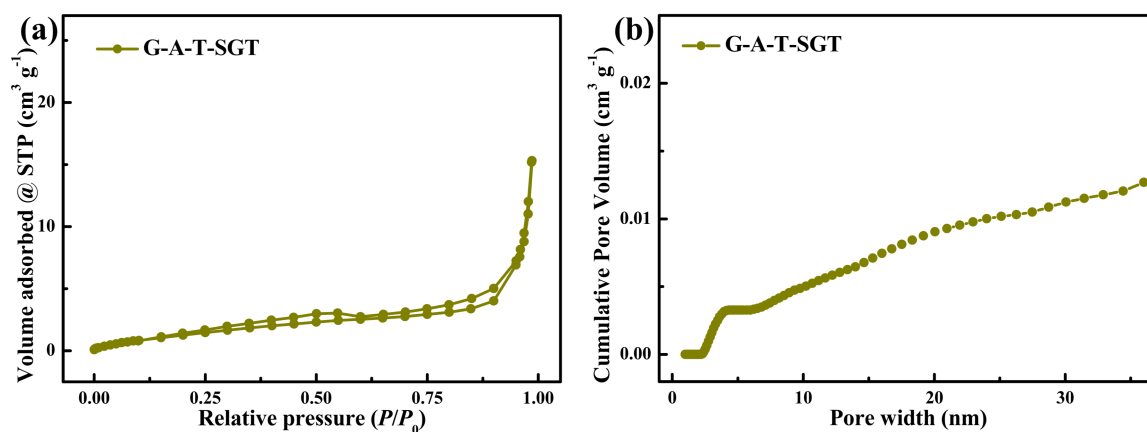


**Fig. S10** (a) N<sub>2</sub> adsorption-desorption isotherm and (b) the cumulative pore volume of G-A-T-SGT.

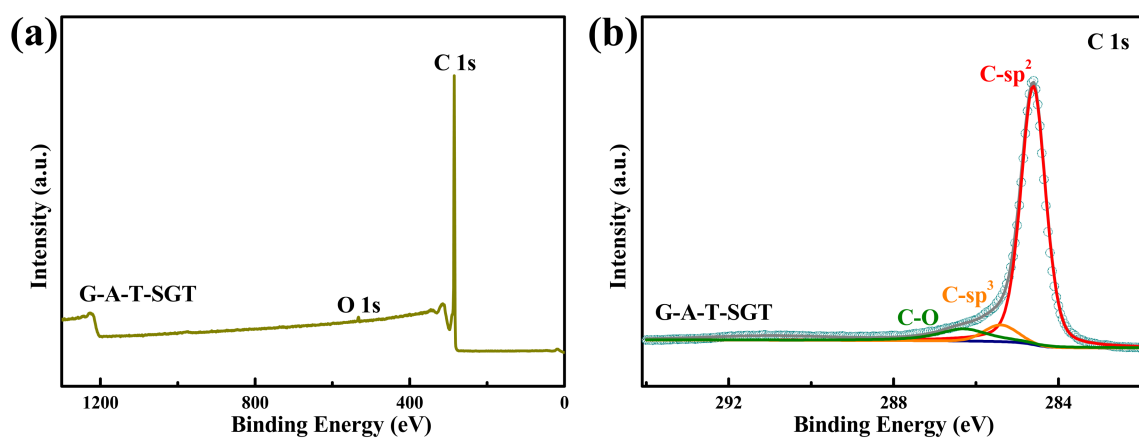


**Fig. S11** (a) Full XPS spectra and (b) high-resolution XPS spectra of C 1s of G-A-T-SGT.

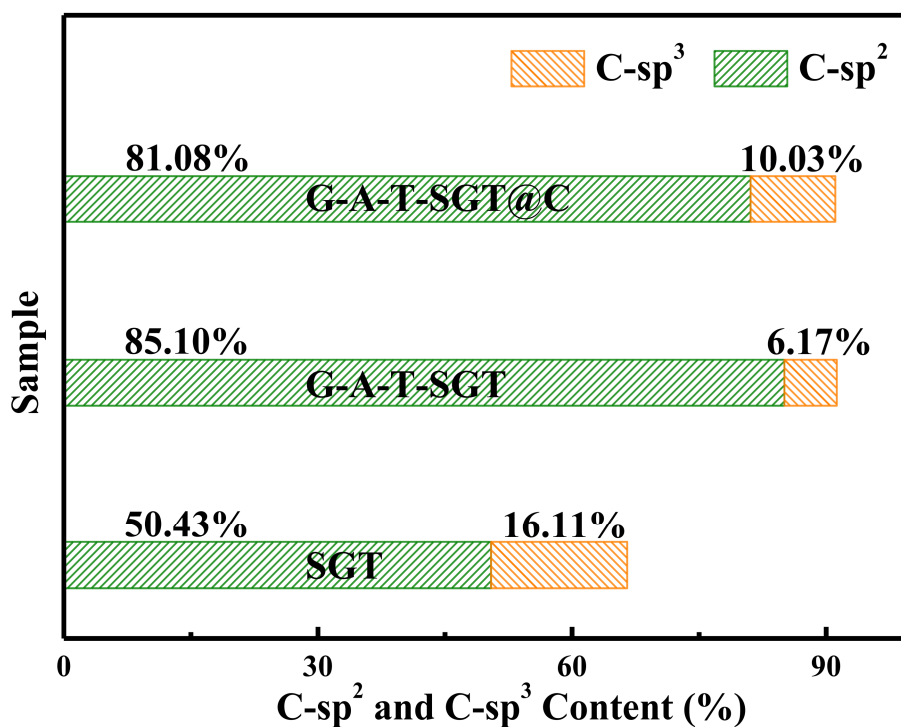


**Fig. S12** The content of C-sp<sup>2</sup> and C-sp<sup>3</sup> in SGT, G-A-T-SGT and G-A-T-SGT@C.

As shown in **Fig. S12**, the content of C-sp<sup>2</sup> on the surface of SGT is only 50.43%, testifying the high defects of SGT which were undergone multiple charge/discharge cycles. And the C-sp<sup>2</sup> content of G-A-T-SGT is more than 85 %, which is really higher than SGT, indicating that the defects especially oxygen defects has been decreased effectively after treatment by graphitization. Furthermore, the content of C-sp<sup>2</sup> (81.08 %) in G-A-T-SGT@C is a little lesser and the C-sp<sup>3</sup> content (10.03 %) is a small higher compared with G-A-T-SGT, which are confirmed the successful coating of amorphous carbon on the surface of G-A-T-SGT.

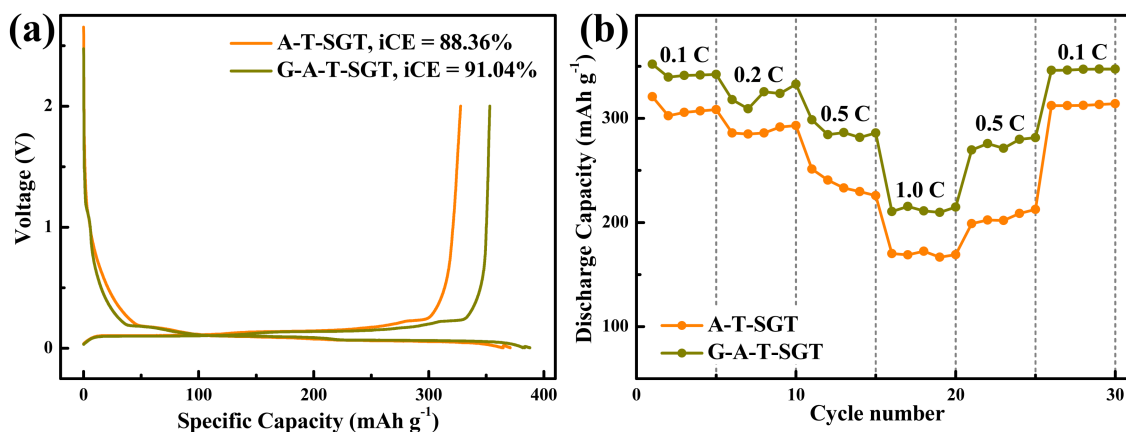


**Fig. S13** (a) Initial charge-discharge curves and (b) the rate capability of A-T-SGT and G-A-T-SGT. (1.0 C = 372 mAh g<sup>-1</sup>)

It can be seen from **Fig. S13a** that the initial coulombic efficiency can reach to 88.36 % of A-T-SGT and 91.04 % of G-A-T-SGT which is much higher than that of SGT (78.84 %). And the rate capability of A-T-SGT and G-A-T-SGT are also superior compared with SGT (**Fig. S13b**).

**Table S1** The  $D_{50}$  and specific surface area of SGT, G-A-T-SGT@C and CGT

Sample	$D_{50} / \mu\text{m}$	Specific Surface Area / $\text{m}^2 \text{g}^{-1}$
SGT	11.25	6.19
G-A-T-SGT@C	14.78	1.29
CGT	14.40	1.06